Journal of Fluids and Structures (1997) **11,** 433–446

ON WIND-INDUCED OSCILLATION OF SAIL-BALLAST SYSTEMS

Takeshi Sugimoto†
Saitama Institute of Technology Okabe, Saitama, 369-02, Japan

(Received 8 November 1996 and in revised form 11 January 1997)

A yacht often rolls very violently when it is sailing down-wind. This divergent oscillation may be dangerous enough to capsize the yacht. This study models a yacht as a sail-ballast system rolling in a wind. A mathematical model is presented to account for this phenomenon. Experiments have also been made for systems with triangular and elliptic sails. Analysis of the nonlinear governing equation implies that the instability occurs owing to coupling effects between aerodynamic and righting moments: in particular the large change in the side force under a small change in the angle of attack. The experimental results support this argument regarding interaction, as well as the existence of three distinctive types of rolling motion: divergence, divergent oscillation, and oscillation with weak damping. Estimated and measured periods of oscillation are in fairly good agreement. Evidence supports the idea that vortices behind the sails are not the main cause of the instability.

1. INTRODUCTION

Down-wind sailing is not always stable. A yacht often exhibits violent rolling, which is self-excited and can capsize the craft. Marchaj (1988; pp. 653–675), a celebrated sailor and yacht–scientist, offered an explanation for this self-excited rolling: (i) the Kármán vortex trail forces initial oscillation; (ii) this oscillation is then amplified by aerodynamic forces. One of the questions is how aerodynamic forces govern the motion. We shall also ask how the ballast at the keel tip affects the oscillation. What sort of equation governs the motion? These questions have not been answered to date.

In order to cast light upon the physics behind the rolling instability, we will introduce a simplified sail–ballast system. Our model is similar to Marchaj's. A system has a sail and a piece of ballast put on a single shaft that can roll in the wind. We have used triangular and elliptic sails. These model systems represent the essential property of the motion. Water and hulls affect down-wind sailing, but we have neglected these effects due to limitations of available facilities. Our model, however, serves as a first approximation to the actual phenomena.

By analysing the model systems theoretically and experimentally, we arrive at a rigorous and sound explanation for the rolling instability of yachts. Our conclusion emphasizes the important role played by the interaction between the aerodynamic forces and the righting moment. The agreement between theoretical and experimental results is fairly good.

In Section 2 we introduce the model system. Section 3 describes the derivation of the equation governing the motion of the system and the analytical characteristics of the associated nonlinear differential equation. Section 4 describes the procedure and

---

† Permanent address: Faculty of Engineering, Kanagawa University, 3-27-1 Rokkakubashi, Kanagawa Ward, Yokohoma, 221, Japan.

0889–9746/97/040433 + 13 $25.00/fl970083

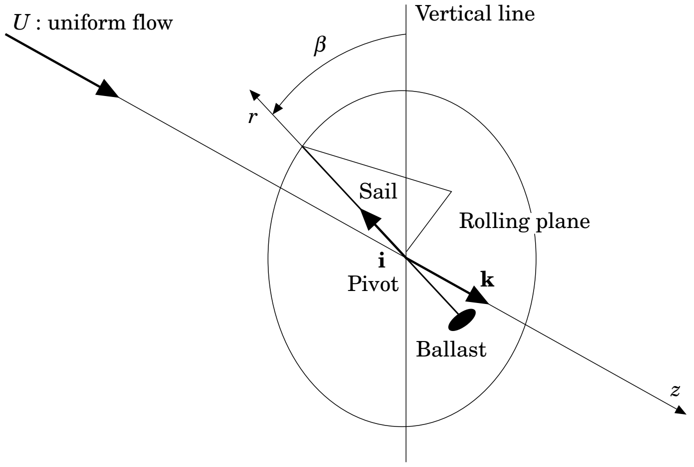

Figure 1. Perspective view of the model system.

apparatus for the experiments. In Section 5 we show and discuss theoretical and experimental results. In Section 6 we summarize our findings.

2. MODEL SYSTEM

The aim of this study is to understand the physics of rolling instability. The main difficulty derives from the complicated geometry of a yacht as well as the existence of two kinds of fluid, i.e., air and water. These characteristics can be circumvented, however. We have modelled a yacht as a sail-ballast system, because this accurately represents the essential configuration of a yacht. Due to limitations of available facilities, we have used conventional wind tunnels only. Therefore our model could not account for the following effects: (a) aerodynamic effects due to mirror images of sails; (b) wind shear developed on the sea surface; (c) hydrodynamic damping due to the hull and keel. These effects are to be studied in the future.

Our model is shown in perspective view in Figure 1 and in the schematic sketch at the top of Figure 2. Instead of a sail, a hull and a keel with ballast in water and air, we adopted a system with a sail and a piece of ballast set upon a single shaft. The system can roll in the plane perpendicular to the wind direction.

3. THEORY

3.1. Equation of Motion

The model and coordinate system (r, β, z) are shown perspectively in Figure 1; r is the coordinate up the mast from the center of rotation; β is a heel angle; and the z coordinate is parallel to the direction of the uniform flow as well as the craft course. The model could swing in the rolling plane, which is perpendicular to z. Swing twists the direction of the relative wind: $U\mathbf{k} + r\dot{\beta}\mathbf{k} \times \mathbf{i}$, where U, $\mathbf{k}$ and $\mathbf{i}$ denote the speed of the uniform flow, the unit vector in the z-direction, and the unit vector in the r-direction, respectively; and a single dot denotes the first derivative with respect to

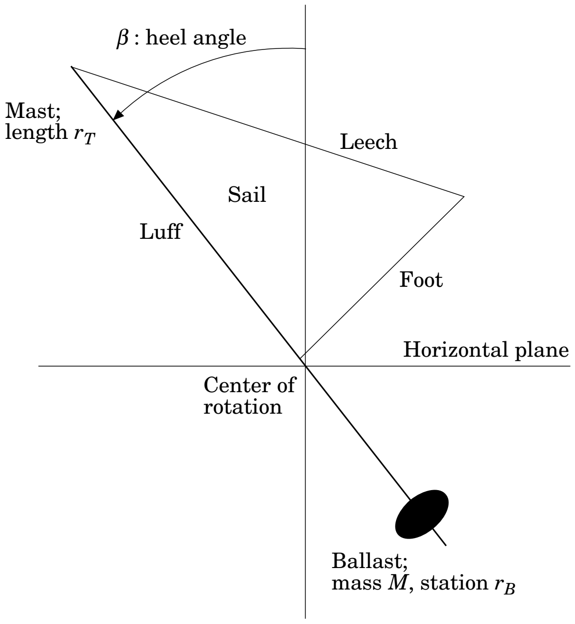

Bow view

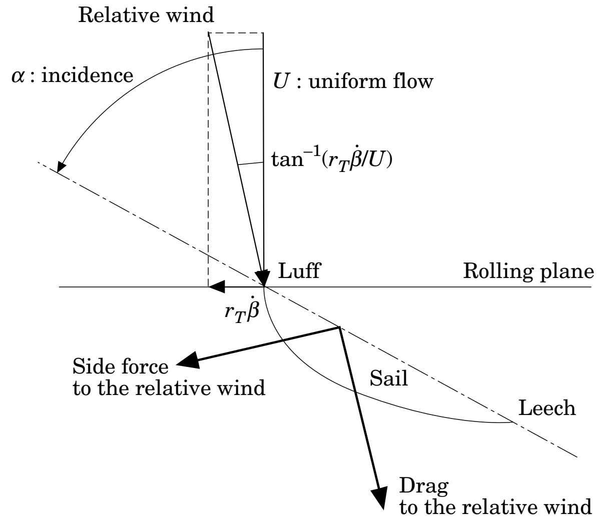

View from the mast top

Figure 2. Nomenclature for the model system.

time. This swing motion is rather slow, as our experiments reveal: a 0·5 m tall sail heels at most 90 degs in a 7·7 m/s wind. The angle between the uniform flow and the relative wind at r is approximated by

$$\arctan(r\dot{\beta}/U) \approx r\dot{\beta}/U \sim \mathcal{O}(0{\cdot}1).$$

From this order estimate, we can deduce that the flow is quasi-steady: we shall neglect any transient aerodynamic effects except the twist of the relative wind mentioned above. Without loss of generality we can also state that three-dimensional effects are included in forces shown at the bottom of Figure 2. The figure describes the force and wind triangles at the sail section looking down from the mast top. Note that all the aerodynamic forces are made nondimensional by dividing by the dynamic pressure times, the chord length or the sail area. Let C_s and C_d be the sectional side force and drag, respectively; then the aerodynamic heeling force assumes the form

$$C_s(\alpha - r\dot{\beta}/U, r)\cos(r\dot{\beta}/U) - C_d(\alpha - r\dot{\beta}/U, r)\sin(r\dot{\beta}/U)$$
$$= C_s(\alpha, r) - C_{s,\alpha}(\alpha, r)r\dot{\beta}/U - C_d(\alpha, r)r\dot{\beta}/U + \mathcal{O}(\dot{\beta}^2),$$

where $C_{s,\alpha}$ denotes the first derivative of C_s with respect to α. We shall neglect higher-order terms than $\dot{\beta}^2$. Integrating this sectional, aerodynamic heeling moment along the mast, we have the equation of motion for the system about the center of rotation, or the origin:

$$(I_0 + Mr_B^2)\ddot{\beta} = \tfrac{1}{2}\rho U^2 S r_T \left\{ \epsilon_1 C_S(\alpha) - [\epsilon_2 C_{S,\alpha}(\alpha) + \epsilon_3 C_D(\alpha)] \frac{r_T}{U}\dot{\beta} \right\} - Mr_B g \sin\beta, \tag{1}$$

where I_0, M, r_B, ρ, S, r_T, C_S and C_D denote, respectively, the moment of inertia with the ballast at the origin, the mass of the ballast, the station of the ballast down from the origin, the air density, the sail area, the mast height, the total side force coefficient, and the total drag coefficient. Denoting the chord length by $c(r)$, aerodynamic coefficients ϵ_1, ϵ_2, and ϵ_3 are defined by

$$C_S(\alpha) = \int_0^{r_T} C_s(\alpha, r)c(r)\,\mathrm{d}r/S, \quad C_{S,\alpha}(\alpha) = \frac{\partial C_S(\alpha)}{\partial \alpha},$$

$$C_D(\alpha) = \int_0^{r_T} C_d(\alpha, r)c(r)\,\mathrm{d}r/S,$$

$$\epsilon_1 = \int_0^{r_T} C_s(\alpha, r)c(r)r\,\mathrm{d}r/\{C_S(\alpha)r_T\},$$

$$\epsilon_2 = \int_0^{r_T} C_{s,\alpha}(\alpha, r)c(r)r^2\,\mathrm{d}r/\{C_{S,\alpha}(\alpha)r_T^2\},$$

and

$$\epsilon_3 = \int_0^{r_T} C_d(\alpha, r)c(r)r^2\,\mathrm{d}r/\{C_D(\alpha)r_T^2\}.$$

Dividing equation (1) by the total moment of inertia, we can rewrite the basic equation as follows:

$$\ddot{\beta} = \tau + (\mu - \nu)\dot{\beta} - \omega^2 \sin\beta, \tag{2}$$

where

$$\tau = \epsilon_1 \frac{\frac{1}{2}\rho U^2 S r_T C_S(\alpha)}{I_0 + Mr_B^2}, \quad \mu = -\epsilon_2 \frac{\frac{1}{2}\rho U S r_T^2 C_{S,\alpha}(\alpha)}{I_0 + Mr_B^2},$$

$$\nu = \epsilon_3 \frac{\frac{1}{2}\rho U S r_T^2 C_D(\alpha)}{I_0 + Mr_B^2} \quad \text{and} \quad \omega = \sqrt{\frac{Mr_B g}{I_0 + Mr_B^2}}.$$

We should note that μ is positive, because $C_{S,\alpha}(\alpha)$ is negative in the down-wind

TABLE 1

Classification for singular points of equation (2)

		$(\mu - \nu)^2 - 4\omega^2 \cos \beta_T$	
		non-negative	negative
$\mu - \nu$	positive	unstable node	unstable focus
	zero		center
	negative	stable node	stable focus

condition. Although equation (2) is equivalent to those studied by Hayes (1953) and Nayfeh & Mook (1979; pp. 131–134), the nature of our equation does not necessarily lead to damped oscillation, unlike in those studies.

3.2. ANALYSIS OF THE GOVERNING EQUATION

Equation (2) has a stationary solution; putting $\ddot{\beta} = \dot{\beta} = 0$, we have the solution

$$\beta_T = \arcsin(\tau\omega^{-2}). \tag{3}$$

In other words, the system may come to equilibrium at $\beta = \beta_T$. It is, however, not known whether this equilibrium is dynamically stable or not.

After the standard procedure given by Nayfeh & Mook (1979; pp. 110–117), we can study the stability of these stationary solutions, or the singular points in mathematical terms.

Examining the Jacobian of equation (2), the nature of the basic equation is summarized by Table 1. The relationships between mathematical terms and kinds of motion are the following: (i) an "unstable node" corresponds to divergent motion without oscillation; (ii) an "unstable focus" corresponds to divergent oscillation; (iii) a "center" corresponds to plane oscillation; (iv) a "stable node" corresponds to convergent motion without oscillation; (v) a "stable focus" corresponds to convergent oscillation. On the basis of Table 1 we can draw the following conclusions.

First we point out that the $\mu - \nu$ term is the key to the stability. The μ term depends on $C_{S,\alpha}$, i.e. the lift-curve slope, while the ν term depends on the drag coefficient C_D. Usually drag does not vary very much in value at $\alpha \approx 90°$. Therefore the rolling becomes unstable, as the lift-curve slope becomes steep.

Another point is the cause of oscillation: motion becomes oscillatory if the $\omega^2 \cos \beta_T$ term becomes larger than the $(\mu - \nu)^2$ term. Since $\beta_T = \arcsin(\tau\omega^{-2})$, oscillation is induced by larger ω and smaller τ. This situation is brought about by the combination of the larger moment of inertia and small side force; this fact leads to estimation of the oscillation period. If ω is much greater than τ and $\mu - \nu$, equation (2) is approximated by

$$\ddot{\beta} \approx -\omega^2 \sin \beta. \tag{4}$$

This is the well-known equation for large-amplitude oscillation of a pendulum. Suppose the initial angular velocity is zero; then the oscillation period, say T, is given by the standard formula [e.g., equation (3.3.74) in Nayfeh & Mook (1979)]

$$T = 2\pi/\omega = 2\pi\sqrt{\frac{I_0}{Mr_B g} + \frac{r_B}{g}}. \tag{5}$$

Another asymptotic form of equation (2) is obtained by letting ω tend to zero. The very small righting moment yields this situation. Neglecting the last term on the right-hand side of equation (2), we obtain

$$\ddot{\beta} \approx \tau + (\mu - \nu)\dot{\beta}. \tag{6}$$

The equation above implies that the motion becomes divergent or convergent without oscillation.

4. EXPERIMENTS

4.1. Force Tests

Figure 3 shows the schematic of the experimental system; the set-up for force tests is shown on the right half of the figure. The smaller sail models were used for the force tests: the length of luff is 0·28 m; the foot length is 0·14 m; the mast length from the root is 0·3 m. The sails are made of a 0·03 mm thick mylar sheet. The Reynolds number was $1{\cdot}3 \times 10^5$ with the wind speed 11·0 m/s. The measurements were made at angles of attack in the range of 90 ± 20 deg by 5 deg increments. We have used a suction-type wind tunnel with closed test-section: its cross-sectional dimensions are 0·6 m × 0·6 m.

Aerodynamic side force, drag, and moment were measured by the use of a cantilever-type force balance. Analog data were digitized and then passed on to the computer.

4.2. Motion Analysis

The set-up is described in the schematic diagram on the left half of Figure 3. The larger sail models were used for the motion analysis: the length of luff is 0·4 m; the foot length is 0·2 m; the mast length from the pivot is 0·5 m. Most parts of the system were made of aluminum. The ballast consisted of a brass circular cylinder of 250 g. Positions of the ballast could be set on the shaft in the range 30–300 mm from the pivot, in 10 mm increments. Both the sail and the ballast are set upon a single shaft. The shaft could roll in the plane perpendicular to the flow at the pivot. Another shaft runs streamwise through this pivot, and is supported by a pair of ball-bearings.

We used a blow-down wind tunnel with open test section. The dimensions of the

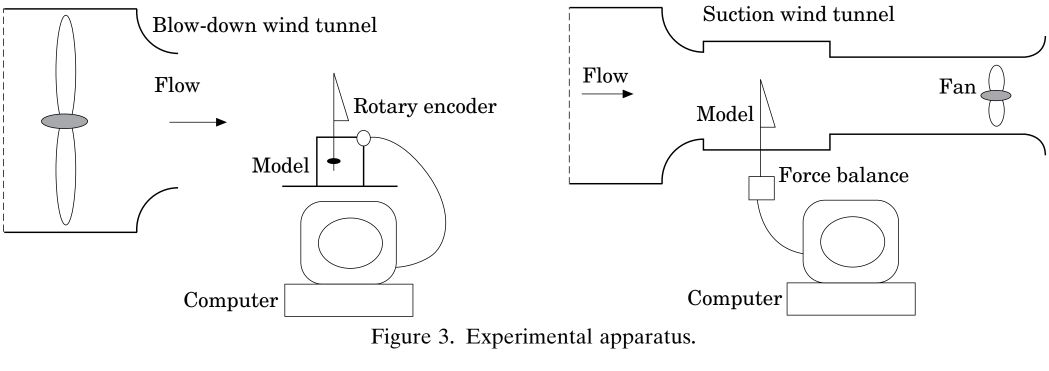

Figure 3. Experimental apparatus.

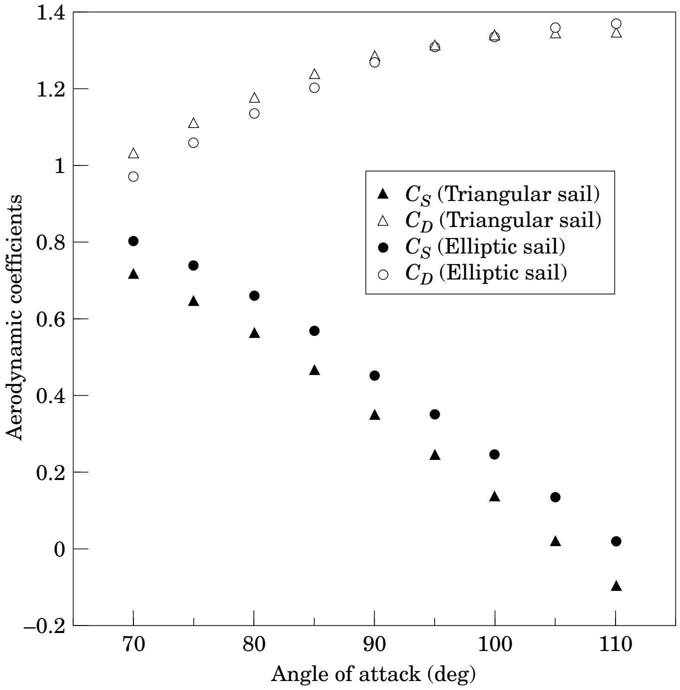

Figure 4. Aerodynamic characteristics of the sails.

outlet are 1·2 m × 1·2 m. The measurements were done at the wind speed of 7·7 m/s, so that the Reynolds number was kept the same as in the force tests, i.e. $1{\cdot}3 \times 10^5$.

The measurements of heel angles were made by the use of an optical rotary-encoder, which could detect an angle as small as 0·45 deg. Analog data were digitized and then passed on to the computer.

We also conducted the flow visualization using the smoke-wire technique.

5. RESULTS AND DISCUSSION

5.1. Aerodynamic Characteristics of Sails

Figure 4 shows the results of the force tests. Both sails have similar aerodynamic characteristics: (i) the side force coefficients change from 0·8 down to around zero; (ii) therefore the slope of the side force coefficients is negative and steep; (iii) changes in drag coefficients are rather small, i.e. from 1·0 up to 1·4. The differences in planforms are summarized in the following: (a) the side force coefficient of the elliptical sail is smaller than that of the triangular sail; (b) the drag coefficient of the elliptic sail is smaller than that of the triangular sail at almost every angle of attack. These differences imply this well-known fact: the high efficiency of the elliptic wing. The presence of the tunnel walls inevitably affects the aerodynamics of the force test models. Therefore, the characteristics of the force test models may differ from those of the sail-ballast systems quantitatively, although qualitative arguments are applicable to both systems in the same manner.

Let us denote the angle of attack, at which the side force vanishes, by the zero-lift angle, designated by α_0. The zero-lift angle of the elliptic sail is about 110 deg; the

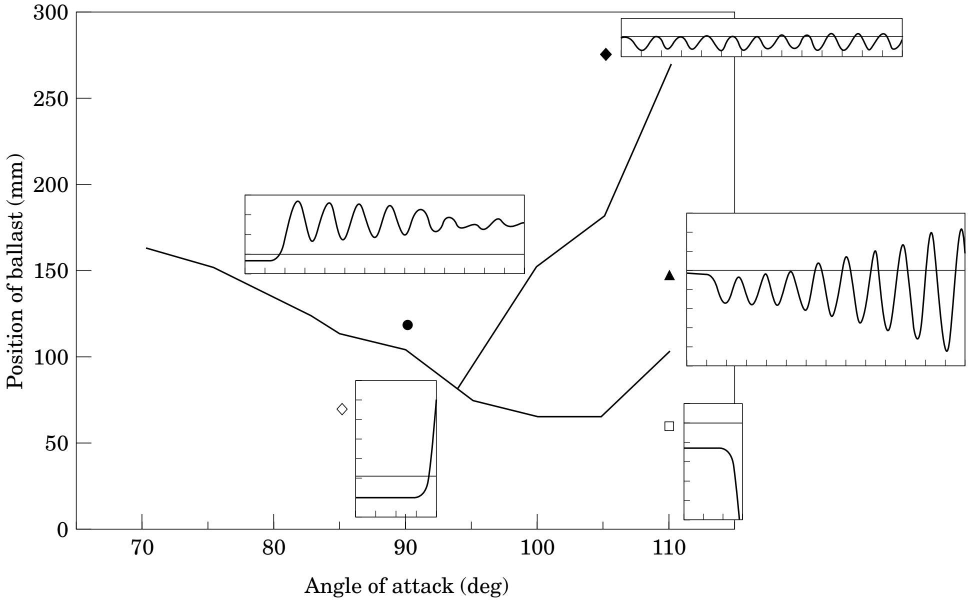

Figure 5. Types of the rolling motion classified in the parameter plane ((α, r_B)) for the triangular sail. Each inset shows typical motion under the corresponding conditions denoted by the adjacent symbol; the abscissa of the inset represents time, and one division corresponds to 1 s; the ordinate of the inset denotes the heel angle, and one division corresponds to 20 deg.

zero-lift angle of the triangular sail is about 105 deg. These angles will be referred to later to annotate the results of the motion analysis.

5.2. Motion of Sail-Ballast Systems

Motion analyses were made under 252 sets of conditions for each model system: (28 ballast positions) × (nine values of angles of attack). Based on the observation and the analysis of heel-angle measurements, we found that motions of each system could be classified into three domains in the parameter plane, i.e. (α, r_B). Figure 5 shows the results of motion analysis for the triangular sail-ballast system, and Figure 6 for the elliptic sail-ballast system. Each inset in these figures shows the typical motion under the corresponding conditions denoted by the adjacent symbol in each domain; the changes in the heel angles are plotted against time. Bold lines represent boundaries between adjacent domains.

The three typical domains correspond to the following: (i) divergent motion without oscillation; (ii) divergent oscillation; (iii) oscillation with weak damping.

The domain of divergent motion is observed if the ballast-pivot distance is small, in the lower portions of Figures 5 and 6. Typical conditions, denoted by open symbols, are the following: $(\alpha, r_B) = (85\,\mathrm{deg}, 70\,\mathrm{mm})$ and $(110\,\mathrm{deg}, 60\,\mathrm{mm})$ in Figure 5; $(\alpha, r_B) = (80\,\mathrm{deg}, 150\,\mathrm{mm})$ and $(105\,\mathrm{deg}, 60\,\mathrm{mm})$ in Figure 6. As shown by insets in these figures, heel angles diverge immediately. If the ballast is set close to the pivot, the righting moment becomes small. This situation is described by equation (6) with the μ term larger than the ν term. According to the results of force tests, it is clear that the slopes of side forces are large. Therefore, for the sail-ballast system, μ is larger than ν. The heeling force, i.e., the aerodynamic side force, becomes smaller as the angle of attack becomes larger. Therefore the border-line goes down in Figures 5 and 6 as the angle of

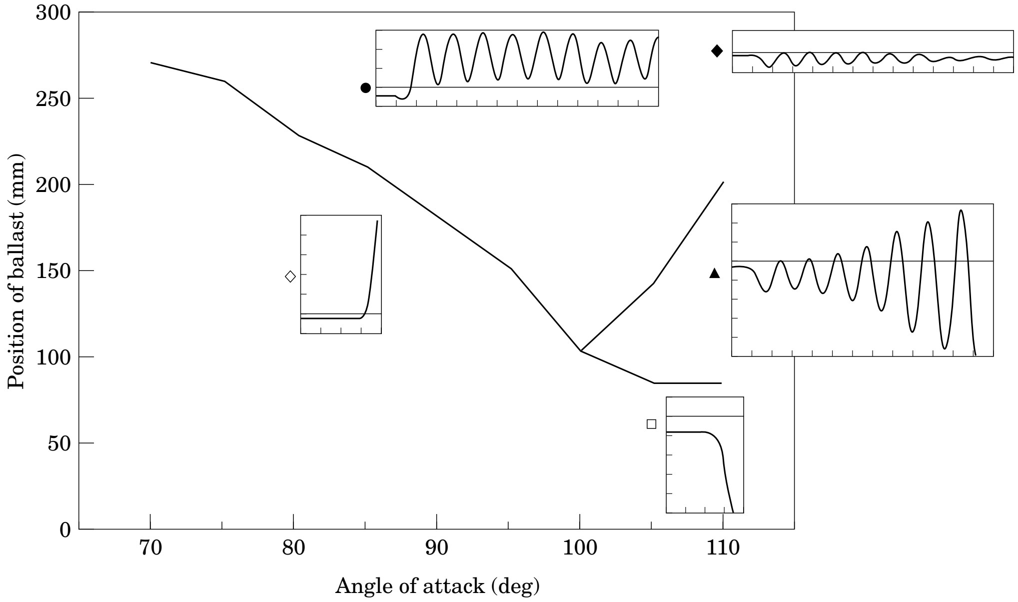

Figure 6. Types of the rolling motion classified in the parameter plane (α, r_B) for the elliptic sail. Each inset shows typical motion under the corresponding conditions denoted by the adjacent symbol; the abscissa of the inset represents time, and one division corresponds to 1 s; the ordinate of the inset denotes the heel angle, and one division corresponds to 20 deg.

attack becomes larger. The turning direction of the heel changes from screw-wise along z direction to counter-screw-wise, as the side force changes its sign at the zero-lift angle.

As stated in the theory section, motion becomes oscillatory with a larger moment of inertia and a smaller side force.

The domain of divergent oscillation occurs under the following conditions: (a) the angle of attack exceeds a certain value; (b) the righting moment is moderate. The former condition is closely related to $C_{S,\alpha}(\alpha)$. The closer the angle of attack comes to the zero-lift angle, the steeper $C_{S,\alpha}(\alpha)$ becomes, as shown by Figure 4. The latter condition corresponds to a situation between those described by equations (4) and (6). Mid-right portions of Figures 5 and 6 correspond to this domain. Typical conditions, denoted by solid triangles, are the following: $(\alpha, r_B) = (110\,\text{deg}, 150\,\text{mm})$ in Figure 5; $(\alpha, r_B) = (110\,\text{deg}, 150\,\text{mm})$ in Figure 6. As shown by insets in these figures, heel angles exhibit divergent oscillation.

The last domain consists of oscillation with very weak damping; in some cases damping effects are so small that oscillation seems purely periodic. The upper portions of Figures 5 and 6 correspond to this domain. Typical conditions, denoted by solid symbols, are the following: $(\alpha, r_B) = (90\,\text{deg}, 120\,\text{mm})$ and $(105\,\text{deg}, 275\,\text{mm})$ for Figure 5; $(\alpha, r_B) = (85\,\text{deg}, 260\,\text{mm})$ and $(110\,\text{deg}, 280\,\text{mm})$ for Figure 6. As shown by insets in these figures, heel angles exhibit oscillation with weak damping. The analysis of heel-angle measurements shows that the strength of damping is not consistently dependent on the parameters α and r_B; the damping varies and the variation is not well explained by these parameters. In other words, the damping occurs rather probabilistically. Therefore, some portion of the damping should be attributed to the irregular forces. The most plausible cause is friction working on the ball-bearings at the pivot. According to the definitions, the τ, μ and ν terms become small as the ballast position r_B becomes large. On the other hand, ω becomes close to unity in the same situation.

Therefore the motion becomes oscillatory and the friction becomes more dominant than the $\mu - \nu$ term in this domain.

5.3. INTRODUCTION OF GOVERNING PARAMETERS

The parameters appearing in Figures 5 and 6 have dimensions. In order to deduce the global conclusion from the results presented in the previous subsection, we shall modify these parameters.

The ballast position r_B corresponds to the strength of the righting moment. Therefore, it is appropriate to replace r_B by the nondimensional righting moment. We can define the nondimensional righting moment, denoted by R, by using the aerodynamic moment; i.e.

$$R = \frac{M r_B g}{\frac{1}{2}\rho U^2 S r_T}. \tag{7}$$

As stated in the theory section, the small side force induces oscillation. Therefore it is natural to reduce the angle of attack by the zero-lift angle, $\alpha - \alpha_0$.

We have plotted boundaries of three domains for both sails in Figure 7: the results of motion analysis in the new parameter plane $(\alpha - \alpha_0, R)$. The coincidence of the lower boundaries, which divide divergent motion from oscillation, is remarkable. We also point out the fact that divergent oscillation occurs in both sails for $\alpha - \alpha_0 \geq -10°$. There is, however, a difference between triangular and elliptic sails with respect to the boundaries between divergent oscillation and weak damping oscillation. The drag coefficient of the elliptic sail is slightly larger than that of the triangular one in the vicinity of the zero-lift angle as shown by Figure 4; therefore a bit stronger damping works for the elliptic sail.

As mentioned above, we believe that there is a possibility of predicting the type of motion for any sail-ballast systems by using these parameters. This idea will be useful at the conceptual design stage of a yacht.

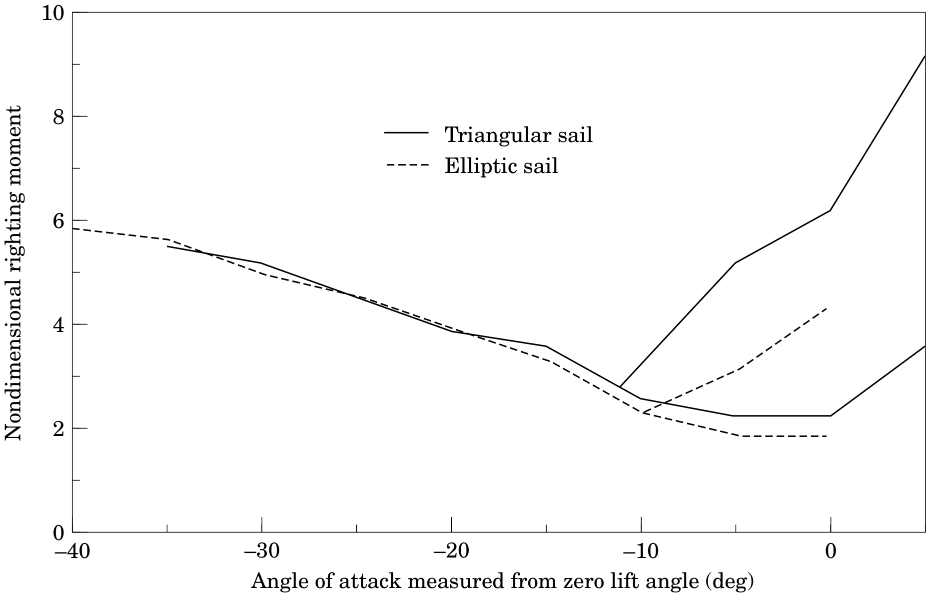

Figure 7. Boundaries dividing the three distinctive type of motion in the parameter plane $(\alpha - \alpha_0, R)$. Bold and dashed lines denote boundaries for the triangular and elliptic sails, respectively.

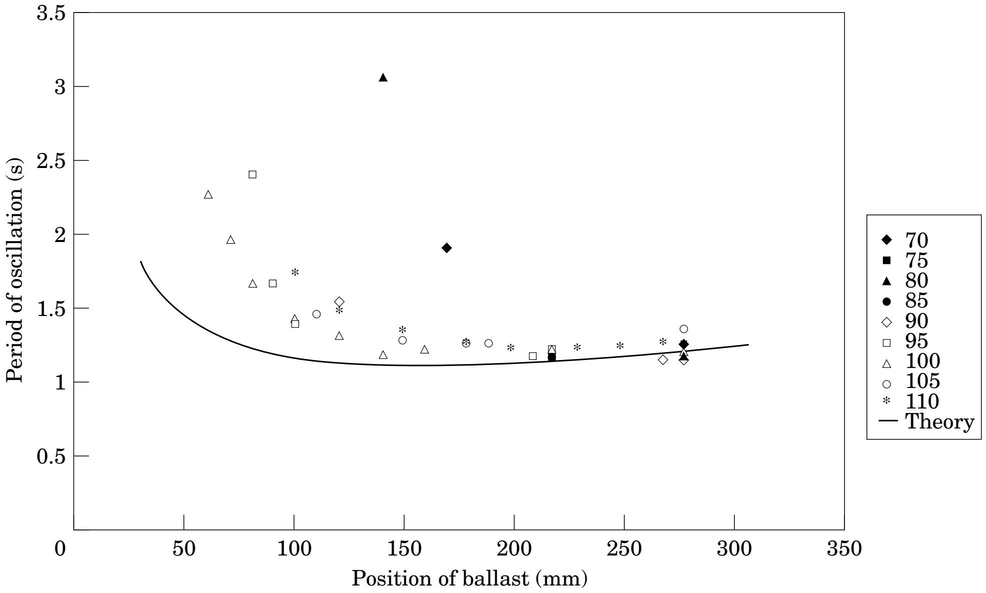

Figure 8. Comparison of oscillation periods between theory [equation (5)] and experiments for the triangular sail.

5.4. Oscillation Periods

We have measured oscillation periods observed in the motion analysis. Let us compare these data with the estimation based on equation (5). Figure 8 shows the results of the comparison for the triangular sail, and Figure 9 shows the results of the comparison for the elliptic sail.

Estimated data are in fairly good agreement with experimental data. This fact assures that our mathematical model describes the essential features of the rolling instability. Although there are some data far from the estimation, these data are taken

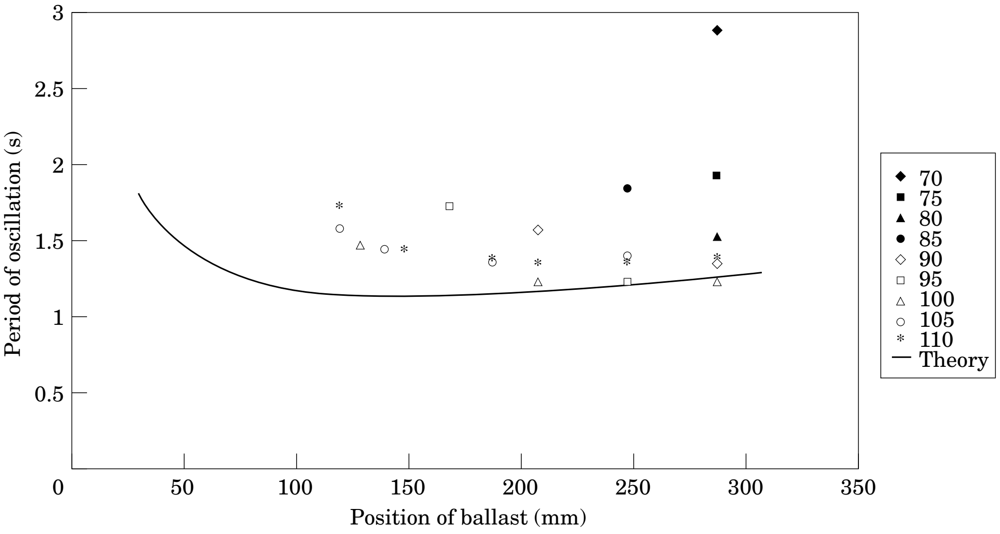

Figure 9. Comparison of oscillation periods between theory [equation (5)] and experiments for the elliptic sail.

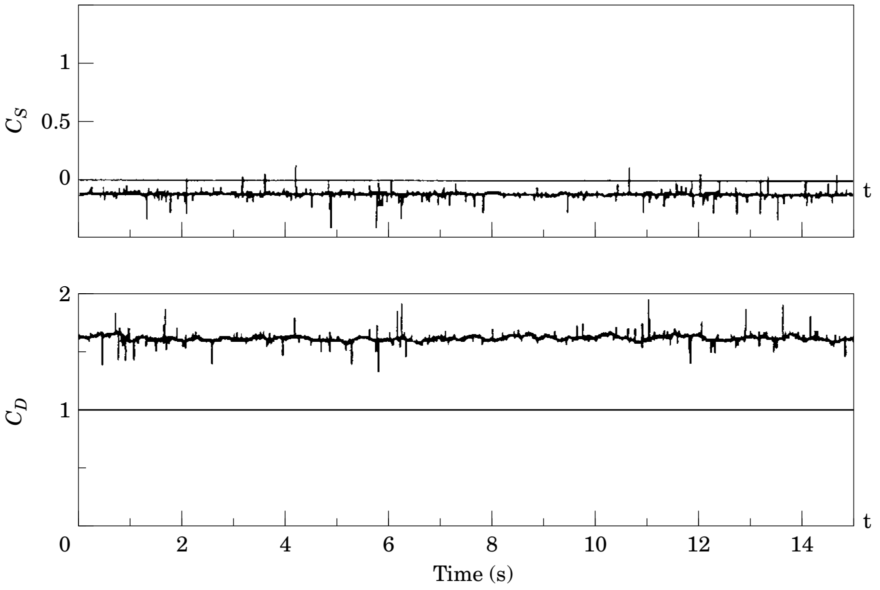

Figure 11. Typical time history of the coefficients of the aerodynamic force acting on the triangular sail fixed in flow at $\alpha = 90°$: C_S for the side force and C_D for the drag.

under conditions very close to the boundary between divergent and oscillatory motion. Therefore, the period becomes longer than for almost pure oscillation.

5.5. Characteristics of Vortex Streets

Figure 10 shows typical examples of flow visualization for the triangular sail fixed in flow. Streak lines revealed the existence of vortices behind the sail. The vortex close to the luff is noticeably larger than the vortex close to the leech, because sails are highly tapered bluff bodies. These asymmetric vortices are also found in flow around the elliptic sail. We are not sure if we can call these asymmetric vortices Kármán vortex streets.

Figure 11 shows the example of the aerodynamic behavior of the triangular sail fixed in flow. According to the motion analysis the oscillation period is around 1–3 s, but the side force does not oscillate over periods of several seconds. Adding to that fact, fluctuations of aerodynamic forces are intermittent and weak. Similar data are obtained for the elliptic sail.

Therefore, vortices behind sails act simply as initial disturbances to start up the rolling motion. As stated above, the stability is governed by interaction between the aerodynamic forces and the righting moment.

Once rolling oscillation occurs, vortices are shed due to the unsteady circulation generation; but these vortices differ from Kármán vortices.

6. CONCLUSIONS

We have conducted a study in simplified sail-ballast models to simulate the rolling motion of a yacht. From the theoretical and experimental results we have drawn the following conclusions.

(1) We have derived the nonlinear equation of motion for the sail-ballast systems.

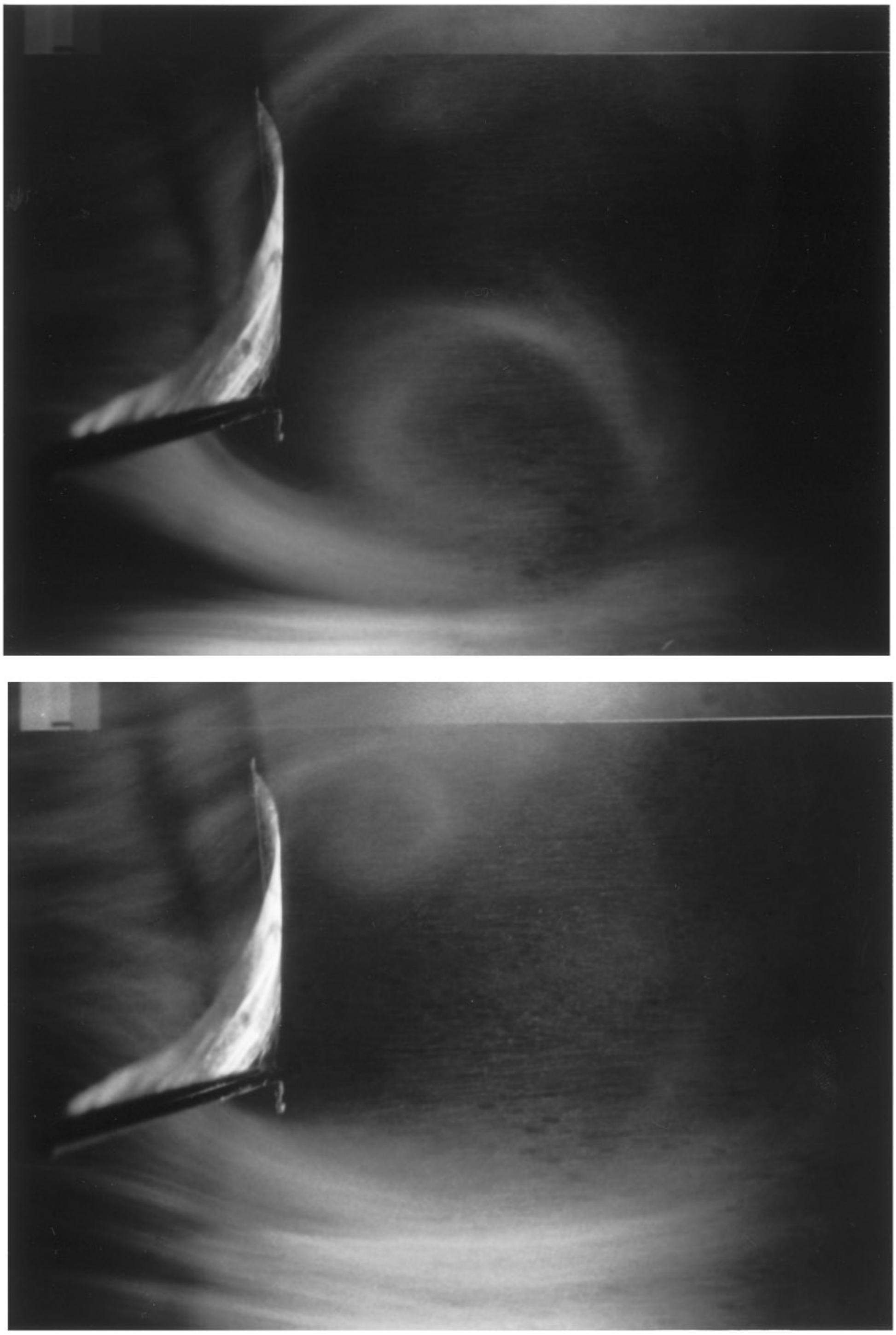

Figure 10. Examples of the flow around the triangular sail. Photos are taken over the mast. The sail is fixed in the flow. The wind is from left to right. The photo at the top shows clearly the large vortex on the luff side (lower part of the photo) and vaguely the small one on the leech side (upper). The photo at the bottom shows clearly the small vortex on the leech side.

This equation describes the essential physics of the rolling instability, i.e. the important interaction between the aerodynamic forces and the righting moment, as well as the instability induced by the steepness of $C_{S,\alpha}(\alpha)$.

(2) Observation revealed three distinct types of motion: divergence, divergent oscillation, and oscillation with weak damping. There exist distinct boundaries that divide adjacent domains of typical motion in the parameter plane (α, r_B). Distribution of these domains can be defined very well on the basis of the governing equation.

(3) By introducing as parameters the nondimensional righting moment R and the angle of attack measured from the zero-lift angle $\alpha - \alpha_0$, the boundaries of motion domains for both triangular and elliptic sail-ballast systems become similar in the parameter plane $(\alpha - \alpha_0, R)$. This suggests the possibility of predicting the type of motion for any sail-ballast system by using these parameters.

(4) Periods estimated by the governing equation are in good agreement with experimental results.

(5) Vortices developed behind fixed sails have small amplitude and shorter periods than the rolling oscillation. Therefore it is natural to think these vortices act only as initial disturbances.

REFERENCES

HAYES, W. D. 1953 On the equation for a damped pendulum under constant torque. *Zeitschrift für angewandte Mathematik und Physik* **4,** 398–401.

MARCHAJ, C. A. 1988 *Aero-Hydrodynamics of Sailing.* London: Adler Coles.

NAYFEH, A. H. & MOOK, D. T. 1979 *Nonlinear Oscillations.* New York: John Wiley & Sons.